Available online at www.sciencedirect.com

ScienceDirect

Procedia Engineering 69 (2014) 758 – 767

Procedia Engineering

www.elsevier.com/locate/procedia

24th DAAAM International Symposium on Intelligent Manufacturing and Automation, 2013

The Deformation Properties of High Strength Steel Sheets for Auto-Body Components

Emil Evin[a]*, Miroslav Tomáš[a], Jozef Kmec[b], Stanislav Németh[a], Branko Katalinic[c], Emil Wessely[d]

[a]*Technical University of Košice, Faculty of Mechanical Engineering, Mäsiarska 74, 040 01 Košice, Slovakia*
[b]*Technical University of Košice, Faculty of Manufacturing Technologies with a seat in Presov, Bayerova 1, 080 01 Presov, Slovakia*
[c]*University of Technology, Faculty of Mechanical and Industrial Engineering, Karlsplatz 13, 1040 Vienna, Austria*
[d] *University of Security Management in Kosice, Kukučínova 17, 040 01, Kosice, Slovakia*

Abstract

The automotive industry requires defining restrictive criteria for prediction of technology characteristics as well as safety characteristics at car's collision with another object when auto-body components are produced from sheet metal blanks. The article presents the methodology for specification the material properties effects to overloading of human organism. Overloading depends on the geometry of the components, on the strain-hardening intensity and limit value of auto-body component's shortening that affect the component deformation path. Proposed criteria are analyzed for the following sheet metal blanks: microalloyed steel H220PD, TRIP steel RAK 40/70, duplex stainless steel, austenitic steel DIN 1.4301 and deep-drawing steel DX 54. The forming limit curves were measured by tensile test performed on the notched specimens with different notch radius.

© 2014 The Authors. Published by Elsevier Ltd. Open access under CC BY-NC-ND license.
Selection and peer-review under responsibility of DAAAM International Vienna

Keywords: material properties; forming limit curve; deformation grid; notched specimen; frontal impact prediction

Nomenclature

E_k	kinetic energy
W_{pl}	deformation work

* Corresponding author. Tel.: +421 55 602 35 47; fax: +421 55 622 51 86.
E-mail address: Emil.Evin@tuke.sk

1877-7058 © 2014 The Authors. Published by Elsevier Ltd. Open access under CC BY-NC-ND license.
Selection and peer-review under responsibility of DAAAM International Vienna
doi:10.1016/j.proeng.2014.03.052

m	weight
v_0	velocity
F	force
ΔL	length change
σ	stress
ε	strain
Re, $R_{p0.2}$	yield strength
Rm	tensile strength
K	material constant
n	strainhardening exponent
$\varepsilon_{0.2\%}$	strain at yield
ε_r	maximum uniform deformation
ΔL_{max}	maximum value of compression or slip of the deformation member
l_i	length of ellipse major axis (referred as 1) and minor axis (referred as 2)
d_k	deformation grid diameter
ε_i	major (referred as 1) and minor (referred as 2) deformation
n_m	number of measurements
a_0	steel sheet thickness

1. Introduction

The ecological requirements arising from the social and legal environment - environmental protection and rational use of mineral resources - need to be combined with the increasing customer demands for car convenience and safety. In order to improve safety, or to reduce the risk of serious and fatal injuries of passengers in case of an accident, there were issued standards as FMVSS 214, EU 96/27/EC and other tests such as SINCAP (Side Impact New Car Assessment Program), NCAP, OFFCAP. When customers buy a car they can use these tests to compare the security features of individual types of cars.

Key criteria for the passenger's survival at collision with another object are: the size of the residual space for passenger's survival (see Fig. 1) and the human body overloading. Every car producer respects the RCAR requirements differently, so we observe different design concepts of auto-body deformation parts. If the car body meets certain amount of protection, components of deformation zones must absorb sufficient kinetic energy during impact.

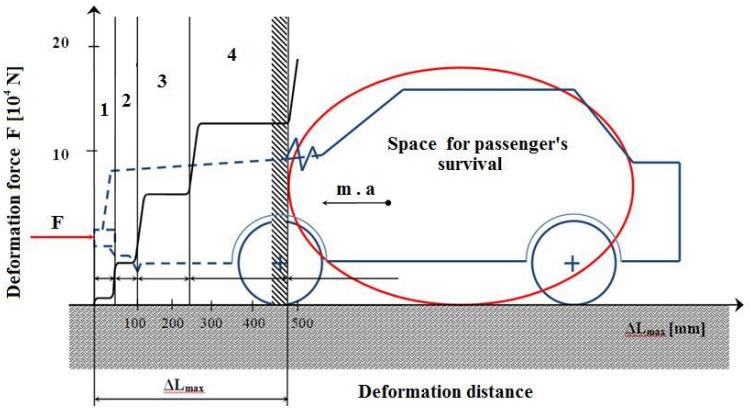

Fig. 1. Simple dynamic model of car at frontal impact to fixed wall
1 – walkers protection, 2 – protection at low velocities, 3 – combining low forces at lower velocities, 4 – deformation at higher velocities.

In order to secure survival of the passengers at collision with another object, it is necessary to prevent collision objects - car components, tree, pole, etc. - from penetrating into the cabin. This means that the cabin space needs to be perfectly tough and strong. Assurance of this requirement depends on the strength and deformation characteristics of carrying auto-body components of auto-body structure. The effectiveness of these components can improve the design of an appropriate structure and appropriate material selection. The structure of the deformation zones components may consist either of several components (parts) of different types of steel sheet or of one component (part) consisting of high strength steel or of several different high-strength steel sheets with different thickness and strength joined by laser welding (tailored blanks) [1, 2, 3, 4, 5].

Materials used in car body structures have to meet wide range of criteria to provide their right application in car production. The most important criterion for auto-body from the view of safety is the ability to absorb energy at impact. The most frequent cases of impact are frontal and lateral impact (Fig. 2) so the auto-body has to be designed to prove absorbing maximum energy and prevent the passenger's threat. For these cases deformation zones are applied in design of auto-body structure. Deformation zones provide as much as possible energy absorption to secure the passenger's space deformation to minimum.

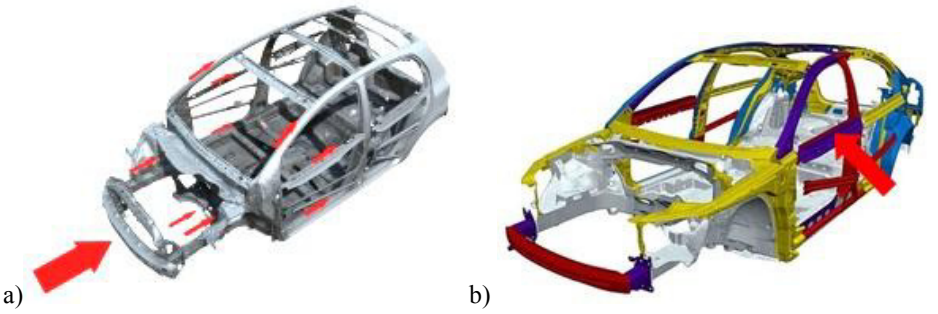

Fig. 2. The energy absorption at frontal (a) and lateral (b) impact.

In the frontal or lateral impacts the auto-body has to absorb a large volume of energy so following requests have to be met by auto-body structure design [6]:

- auto-body must be met the strong impact without tearing or fracture,
- deformation zones must be designed to lead the whole energy not into the passenger's space but to "runaround" the auto-body,
- the engine if placed in the front must move at frontal impact below the car and not into the driver's space,
- any auto-body parts are not allowed to fly away from structure at impact no matter how large they are,
- the doors at lateral impact must work to open.

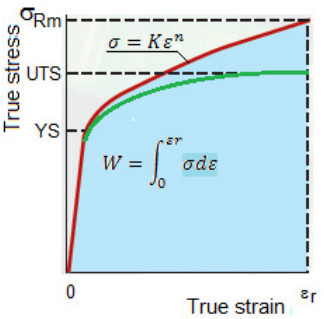

Fig. 3. True stress-true strain dependence.

At the paper, the attention has been focused on conditions of the human body overloading (vehicle deceleration at impact) at frontal collision. When defining criteria for selection of the material, it is possible in this case to assume that the kinetic energy E_k at the moment of impact is equal to the deformation work W_{pl} – see Fig. 3 [6,7,8].

$$E_k = W_{pl} \tag{1}$$

or

$$\frac{1}{2}.m.v_0^2 = \int_0^{\Delta L\max} F(\Delta L, \Delta v)\,\Delta L \tag{2}$$

If we express the deformation work from the tensile test diagram of dependence true stress-true strain as the area under the curve of true stress-true strain, we get:

$$W_{pl} = V_0 \frac{K.\left(\varepsilon_r - \varepsilon_{0.2\%}\right)^{n+1}}{n+1} = F.\Delta L_{\max} = m.a.\Delta L_{\max} \tag{3}$$

After adjustment of the equation (3) we obtain deceleration (overloading), depending on the dimensions and material properties of components for the frontal impact deformation zone as follows:

$$a_i = V_0 \frac{K.\left(\varepsilon_r - \varepsilon_{0.2\%}\right)^{n+1}}{m.\left(n+1\right).\varepsilon_r.\Delta L_{\max}} \tag{4}$$

When compression of deformation members to the value greater than ΔL_{max}, than the loss of the stability (contraction, resp. fracture) occurs in critical points of the deformation member at the frontal impact zone as well as impact of stronger and tougher components (engine, transmission, etc.) of vehicle to barrier occurs. The critical value ΔL_{max} of compression of deformation members in a plane deformation state can be determined from the maximum uniform strain (FLD0) in deformation $\varepsilon_2 = 0$ as follows [9, 10, 11]:

$$\Delta L_{\max} = FLD0.L_0 \tag{5}$$

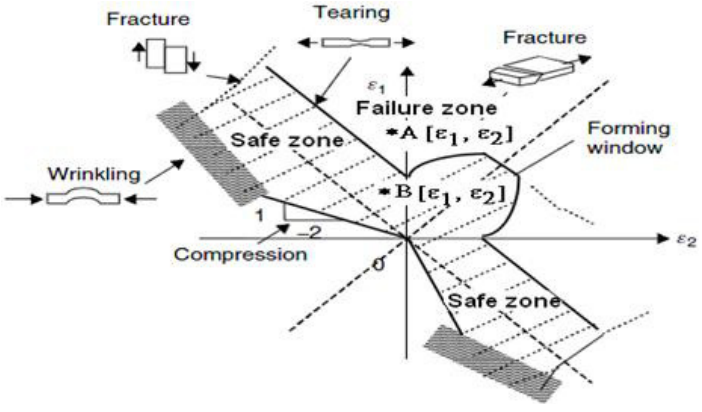

a)

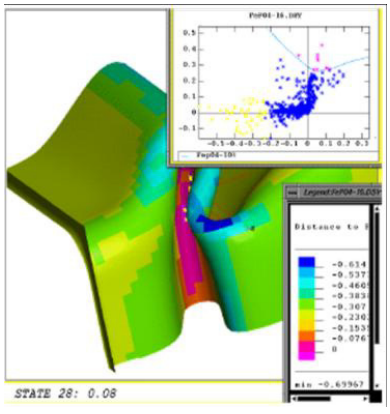

b)

Fig. 4. Forming limit diagram [9] – (a) and result of FEM simulation of beam compression – (b).

2. Experimental research program

For experimental research aimed on determination of the forming limit curve following types of steel sheets were used and referred in the text as follows:

- A - micro-alloyed steel sheet H220PD + Z100MBO,
- B - TRIP steel sheet RAK 40/70 + Z100MBO,
- C - duplex stainless steel,
- D - austenitic steel sheet DIN 1.4301,
- E - galvanized deep drawing quality steel sheet DX 54 D.

Material properties: yield strength, modulus of elasticity, material constant, strain hardening exponent, the maximum uniform strain and forming limit curves were determined by tensile test in accordance with ISO 6892-1, ISO 10113:2006 (coefficient of normal anisotropy test) and ISO 10275: 2007 (strain hardening exponent test).

Forming limit curves of investigated materials were experimentally determined by tensile test with following notch radiuses on specimens r = 2 mm, r = 15 mm, r = 25 mm - Fig. 5. By changing notch radius we modeled various loading conditions that were necessary for constructing the left side of the diagram of forming limit curves. Notch radiuses on specimens were made by electro-discharge wire cutting method. The circle deformation grid with diameter of 2 mm was applied to the specimen's surface by electrochemical etching.

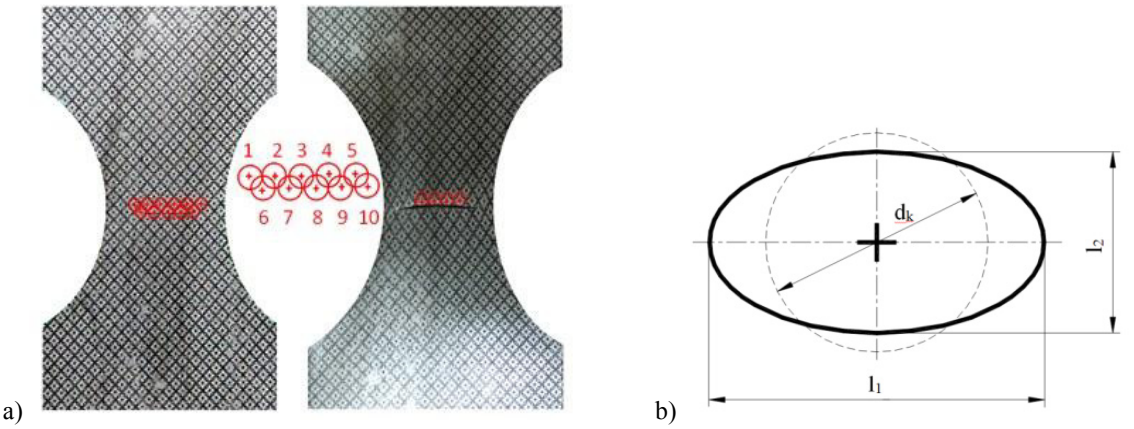

Fig. 5. Specimen with deformation grid before (left) and after (right) deformation – (a) and evaluation of deformed grid elements – (b).

In order to determine the beginning of contraction accurately and objectively, we have captured whole test at CCD camera. Dimensional changes of the deformation grid before and after deformation were evaluated. Grids lying side by side in ten locations of fracture were evaluated before deformation and after deformation, from the video recording of the deformation grid, using routine programmed in Matlab software. The average strain values ε_1 and ε_2 in the plane of the steel sheet and standard deviation – STDEV were calculated from measured results using equations:

$$\varepsilon_1 = \frac{l_1 - d_k}{d_k} \tag{6}$$

$$\varepsilon_2 = \frac{l_2 - d_k}{d_k} \tag{7}$$

$$STDEV = \sqrt{\frac{\sum(\varepsilon_i - \bar{\varepsilon})^2}{n_m}} \tag{8}$$

As mentioned above, in the case of frontal impact, if local narrowing occurs then there is plastic instability on the ultimate tensile strength $\varepsilon_{1r,\ max}$. In critical points of deformation members, when rigid components of vehicle (engine, transmission, etc.) impact on barrier, great overloading of human body occurs.

Keeler and Brazier [10, 12] proposed an empirical relationship for prediction of the critical value of deformation ε_{10}, or FLD0 for plane stress-strain state (ε_2=0):

$$\varepsilon_{10} = FLD0 = (23.3 + 14.3a_0)\frac{n}{0.21} \tag{9}$$

FLD0 value was also determined as an intersection of the experimentally measured deformation ε_{1max} depending on the deformation ε_2 in deformation $\varepsilon_2 = 0$. The results of computed and experimentally measured FLD0 are shown in the Tab. 2.

For $\varepsilon_2 < 0$ the curve on the left of the forming limit diagram is calculated:

$$\varepsilon_{1L} = FLD0 - \varepsilon_2 \tag{10}$$

If we assume that the structure and geometry of the components of deformation zones are the same, then the requirements to the vehicle safety and environmental requirements can be varied by material composition of automotive components. Then during material innovation, the human body overload at assumed ratio $c_1.V_0/m = 1$ can be expressed by the relation (4) only by use of material properties as follows:

$$\Delta a_i = 1.\frac{K.(\varepsilon_r - \varepsilon_{0.2\%})^{n+1}}{(n+1).\ \varepsilon_r.\Delta L_{\max}} \tag{11}$$

In order to compare ability of materials to absorb deformation work at impact, bending test of specimens was done. The strips width was 38 mm and the force and distance were measured until the fracture occurs. The strip ends were fixed by jaws. Based on eq. 2, the deformation work has been computed by numeric integration of force-displacement records. The test configuration is shown in Fig. 6.

Fig. 6. Bendig test of strips.

3. Reached results and discussion

Measured values of material properties for experimental materials are shown in Tab. 1. The results of experimentally measured values of major ε_1 and minor ε_2 deformations on notched specimens as well as the results of computed and experimentally measured FLD0 are shown in the Tab. 2. The principle of the left part of forming limit curve determination for experimental materials B and D is shown in Fig. 7.

Table 1. Measured mechanical properties of experimental materials.

	Material	Direction [°]	$R_{p0,2}$ [MPa]	Rm [MPa]	A_{80} [%]	K	r	n	$\varepsilon_{1,r\,max}$
A	Micro-alloyed steel H220PD	90°	223	368	38	648	1.57	0.230	0.23
		STDEV	2	4	1	10	0.08	0.002	0.01
B	TRIP steel RAK 40/70	90°	434	751	31	1408	0.72	0.285	0.26
		STDEV	1	4	1	5	0.040	0.001	0.01
C	Duplex stainless steel	90°	327	492	30	856	1.02	0.204	0.19
		STDEV	1	3	2	5	0.01	0.001	0.01
D	Austenitic steel DIN 1.4301	90°	305	750	68	1614	0.945	0.491	0.60
		STDEV	7	2	1	8	0.006	0.009	0.01
E	Deep drawing quality steel DX 54 D	90°	169	280	47	469	1.25	0.24	0.26
		STDEV	1	2	1	5	0.07	0.002	0.01

Table 2. Measured values of major and minor deformations on notched specimens and calculated values of FLD0.

	Material	Deformation in plane	Notch radii R 2 [mm]	R15 [mm]	R25 [mm]	STDEV	FLD0	FLD0 calculated by eq. (9)
A	Micro-alloyed steel H220PD	ε_1	0.22	0.3	0.31	0.03	0.2	0.39
		ε_2	-0.02	-0.07	-0.1	0,01	0	0
B	TRIP steel RAK 40/70	ε_1	0.18	0.25	0.26	0,03	0.19	0.47
		ε_2	-0.018	-0.06	-0.07	0,01	0	0
C	Duplex stainless steel	ε_1	0.21	0.29	0.30	0.03	0.2	0.33
		ε_2	-0.01	-0.08	-0.11	0.01	0	0
D	Austenitic steel DIN 1.4301	ε_1	0.54	0.77	0.82	0.03	0.49	0.81
		ε_2	-0.028	-0.17	-0.20	0.01	0	0
E	Deep drawing quality steel DX 54 D	ε_1	0.49	0.43	0.35	0.04	0.32	0.4
		ε_2	-0.2	-0.13	-0.04	0.1	0	0

Comparing measured and calculated values of FLC0 for experimental material it is shown the largest FLD0 value was recorded for the material D – austenitic steel and the lowest for the material C – duplex stainless steel. There is also a difference in measured and calculated values of FLC0 for each material. The relationships (9) and (10) are used in numerical simulations to predict limit deformations in a steel sheet plane and in the thickness direction. From the equation (9) follows the relationship specifies the position FLD0 depending on strainhardening exponent and the sheet thickness. The achieved results suggest that significantly greater differences in calculated and measured values exist in the case of unstable austenitic steels with TRIP effect and austenitic steel DIN 1.4301 - Tab. 2.

The accuracy of the FLD0 and forming limit diagram prediction for deformation states with $\varepsilon_2 < 0$ affects the accuracy of results of numerical simulations for crash tests and also formability of the sheet. It follows from the equation (9) that position of FLD0 depends on the strainhardening exponent and on the sheet thickness. Strainhardening exponent in materials with TRIP effect is not constant throughout the interval of uniform plastic deformation. Therefore, it is necessary to analyze the relationship very precisely.

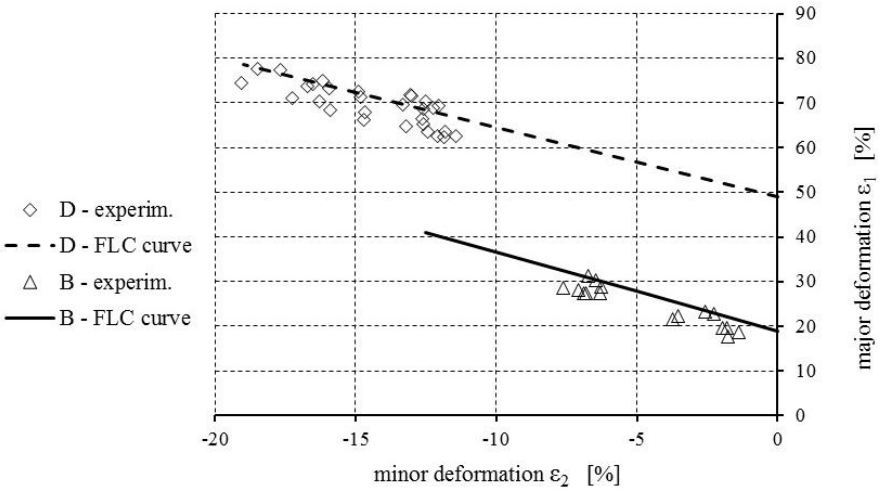

Fig. 7. Experimentally measured left part of forming limit curve.

Based on eq. (11) the contribution of unit deceleration Δa_i for each experimental material was calculated. From comparison of deceleration contribution Δa_i courses (Fig. 8) we can see that during frontal collision components made of drawing quality steel and austenitic steel DIN 1.403 show a lower increase of human body overloading, while TRIP steel shows a rapid increase of human body overloading. Thus, we concluded that austenitic steels and TWIP steels are more appropriate for components of a frontal collision zones than TRIP steels in view of human body overloading during frontal collision.

Strain rate during a frontal collision is different than at the static tensile test. Thus, it is necessary to include into the relations used for prediction of the deformation limit also the index "m" of sensitivity to the strain rate.

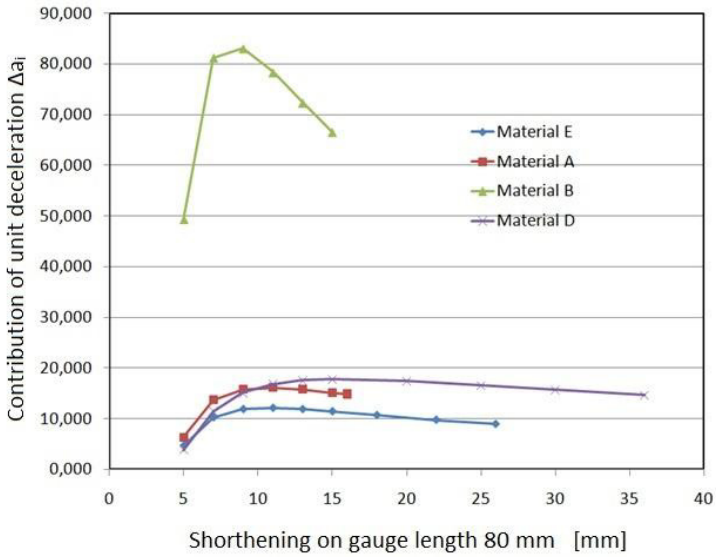

Fig. 8. The dependance of deceleration contribution Δa_i on length.

As it comes out from the presented results, austenitic steel has good ability to absorb energy and deceleration and they can be used for production of deformation zone parts at frontal impact zone as well.

The results of bending test are shown in Fig. 9 and in Tab. 3. From measured and calculated values of deformation work comes out the best deformation ability has austenitic steel DIN 1.4301 and the worst TRIP steel. The most intensive increasing of deformation force was also recorded for TRIP steel. Therefore, it is assumed the highest overloading of human organism in initial phase of impact. This knowledge is confirmed by Fig. 8 as well.

Table 3.. Computed values of deformation work.

	Material	Max. force [kN]	Bending punch travel to fracture [mm]	Deformation work at bending test W_{pl} [Nm]	Deformation work at tensile test acc.to Eq. (3) [Nm]
A	Micro-alloyed steel H220PD	16.08	44.49	327.8	109
B	TRIP steel RAK 40/70	23.88	34.50	313	246
C	Duplex stainless steel	19.59	43.53	385.5	122
D	Austenitic steel DIN 1.4301	40.67	47.07	1448.1	627
E	Deep drawing quality steel DX 54 D	13.83	61.86	402.9	90

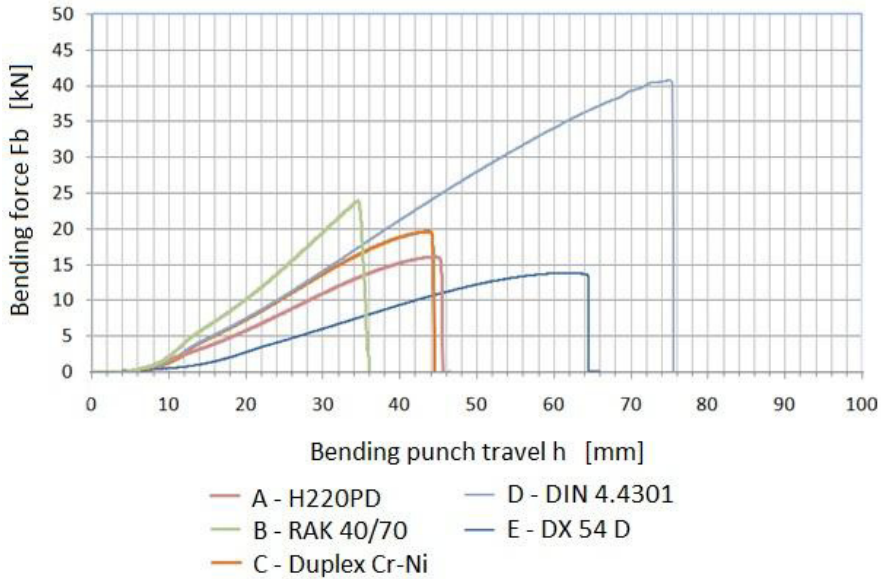

Fig. 9. The force-distance records at bending test.

4. Conclusion

The materials used in the car body offer the highest potential for improvement. High strength steel has been specifically developed by the steel industry to fulfill the demands of the automotive industry. High strength steels can provide the required mechanical properties at low cost and with a low environmental impact. Based on realized experiments, measurements and calculations, achieved results can be summarized as follows:

1. The largest FLD0 value measured by tensile test of notched specimens was recorded for the material D – austenitic steel and the lowest one for the material C – duplex stainless steel.
2. The largest FLD0 value calculated by Keeler and Brazier eq. (9) was recorded for the material D – austenitic steel and the lowest one for the material C – duplex steel. The relation (9) specifies the position FLD0 depending on strainhardening exponent and the sheet thickness. The relation is preferable for drawing quality steels as it is not suitable to predict limit deformation FLD0 for AHSS steels.
3. Significantly greater differences in calculated and measured values exist in the case of unstable austenitic steels with TRIP effect and austenitic steel DIN 1.4301.
4. Based on calculation the contribution of unit deceleration Δa_i according to eq. (11), auto-body components made of drawing quality steel DX 54 D and austenitic steel DIN 1.403 show a lower deceleration, i.e. increase of human body overloading, so they are more appropriate for components of a frontal collision zones than TRIP steels.
5. The best deformation ability to absorb deformation work during collision has austenitic steel DIN 1.4301 and the worst TRIP steel as it has been confirmed by bending test of strips with fixed ends. Austenitic steel presented a larger amount of induced martensite even at low deformations, resulting in hardening of material, and less contribution of the TRIP effect [13].

Acknowledgements

Authors express their thanks for project VEGA 1/0824/12 supported by Scientific Grant Agency of the Ministry of Education, Science and Research of Slovakia and APVV-0273-12 supported by Slovak Research and Development Agency.

References

[1] G. Davies, Materials for Automobile Bodies, 1st ed., Elsevier, Oxford, 2003.
[2] R. Čada, Formability of steel sheets, 1st ed., Repronis, Ostrava, 2001.
[3] P. Doubek, L. Kovárik, P. Solfronk, M. Kolnerová, Distribution of deformations around the fracture of brittle materials at single-axis loading, In: International scientific conference at 55 anniversary of Faculty of mechanical engineering foundation, TU Ostrava, 2005.
[4] W. F. Hosford, R. M. Caddel, Metal Forming - Mechanics and Metallurgy, 3rd ed., Prentice Hall, Engelwood Cliffs, 2007.
[5] G. W. Bright et all, Variability in the mechanical properties and processing conditions of a High Strength Low Alloy steel. Procedia Engineering, Vol. 10, 2011, p. 106-111.
[6] R. Burdzik, P. Folęga, Ł. Konieczny, B. Łazarz, Z. Stanik, J. Warczek, Analysis of material deformation work measures in determination of a vehicle's collision speed, Archives of materials Science and Engineering, Vol. 58, No.1, 2012, pp13-21.
[7] E. R. H. Fuchs, D. R. Field, R. Roth, R. E. Kirchain, Strategic materials selection in the automobile body:Economic opportunities for polymer composite design. Composites science and technology, Vol. 68, No. 9, 2008, pp.1989-2002.
[8] E. Evin, Design of dual phase steel sheets for auto body. Acta Mechanica Slovaca, Vol. 15, No. 2, 2011, pp. 42-48.
[9] J. A. H. Ramaekers, A Criterion for Local Necking, In.: 6th Shemet, Vol. 2, 1998, p. 343-354.
[10] S. P. Keeler, W. G. Brazier, Relationship between Laboratory Material Characterization and Press-Shop Formability, In. Microalloying 75, pp. 517-530.
[11] H. Liu, J. Chen, M. Xiao, Modeling and Simulation of Joint Zone for Stability Analysis of Underground Excavation Engineering. Procedia Engineering, Vol. 37, 2012, p. 1-6.
[12] E. Evin, M. Tomáš, Comparison of Deformation Properties of Steel Sheets for Car Body Parts. Procedia Engineering, Vol. 48, 2012, p. 115-122.
[13] M. Nakajima et all, Effect of quantity of martensitic transformation on fatigue behavior in type 304 stainless steel. Procedia Engineering, Vol. 10, 2011, p. 299-304.